Renewable Energy 235 (2024) 121276

Contents lists available at ScienceDirect

Renewable Energy

journal homepage: www.elsevier.com/locate/renene

Low-voltage DC collection grids for marine current energy converters: Design and simulations

Christoffer Fjellstedt *, Johan Forslund, Karin Thomas

Division of Electricity, Department of Electrical Engineering, Uppsala University, Lägerhyddsvägen 1, Uppsala, 752 37, Sweden

ARTICLE INFO

Keywords:
Marine current energy
DC collection grids
Simulations

ABSTRACT

Marine current energy represents a globally abundant yet largely untapped renewable energy source, offering greater predictability than other sources such as wind. Consequently, it has the potential to play a vital role in the green transition. A critical consideration for harnessing marine current energy is the design of the electrical grid to accommodate multiple turbines. Therefore, this paper presents a study that explores three types of DC collection grids (series, parallel, and star) for a specific marine current energy converter. A simulation model developed for the marine current energy converter is introduced and utilized to assess these topologies for grids comprising ten identical turbines subjected to varying water speeds. The designed topologies are intended for low-voltage and nearshore applications. The simulation results demonstrate that the series collection grid requires a significantly higher DC grid voltage compared to the other topologies for the turbines to operate correctly. Additionally, the study reveals that all three grid topologies can effectively transmit power to the distribution grid with similar power losses.

1. Introduction

The growing demand for renewable energy has heightened interest in alternative green energy sources, including marine energy. Marine currents, in particular, demonstrate greater predictability compared to other green energy sources like the wind or the sun [1,2]. Moreover, they represent a globally abundant and largely untapped resource [3]. Consequently, marine current energy has the potential to play a significant role in the modern green energy system.

Currently, the number of commercial marine current energy projects is still limited. The existing projects today are mainly of a demonstrative nature and based on single devices [4]. The only existing array of marine current energy converters (MCEC) is reportedly the EnFAIT project, where six turbines are placed in an array in the waters outside Shetland in Scotland [5]. Moreover, two of the turbines are connected to an offshore hub, from which the power is transmitted to the shore via a single cable. The system is grid-connected and has delivered power to the grid.

Six turbines in an array are still very minor compared to offshore wind power, where wind farms with hundreds of turbines have been constructed; see, for example, Refs. [6–8]. The trend in offshore wind is for larger turbines and farms located further away from the shore [7,8]. Reasons for this are that the winds are more stable further out at sea, and there is an abundance of free space.

As marine current energy is further developed and commercialized, it is reasonable to believe that larger arrays of turbines will be considered. An obvious benefit of collocating multiple turbines is that more power can be supplied to the electrical grid. Moreover, an array can also be beneficial from the perspective of an efficient use of resources since multiple turbines can share the same infrastructure, such as cables.

To enable the construction of arrays of MCECs, it must be considered how the internal electrical grid in the farm is constructed and how the power is transmitted to the shore and, finally, injected into the distribution grid. The standard technology in offshore wind is alternating current (AC) systems [7,9]. However, as larger wind farms located further from the shore have been commissioned, high-voltage direct current (HVDC) has been considered and used for power transmission to the shore [10]. Systems based on DC collection grids for offshore wind power have been considered in the literature; for example, Refs. [11–15]. However, to the knowledge of the authors, there are no large-scale collection grids based on DC technologies. A power collection system based on DC technology can be beneficial since losses can be decreased, components can be made smaller, and fewer cables are needed [16].

The research into collection grids for marine current energy is still very minor. Electrical systems and array networks for marine energy

* Corresponding author.
E-mail addresses: christoffer.fjellstedt@angstrom.uu.se (C. Fjellstedt), johan.forslund@angstrom.uu.se (J. Forslund), karin.thomas@uu.se (K. Thomas).

https://doi.org/10.1016/j.renene.2024.121276
Received 1 February 2024; Received in revised form 6 August 2024; Accepted 30 August 2024
Available online 2 September 2024

have been investigated from a general perspective in three reports from ORE Catapult [17–19]. A techno-economic review of electrical components for marine energy is given in [20]. Therefore, in order to deepen the knowledge of collection grids for MCECs, the study presented in this paper investigates low-voltage nearshore DC collection grids for a MCEC. Since there is a lot of research and commercialized examples of AC grids for offshore wind power, only DC grids are considered in this paper. Furthermore, the choice of DC collection grids is motivated by the fact that fewer cables are needed, and components can potentially be made smaller. These factors can be especially beneficial in marine current energy applications, where turbines are typically located beneath the water surface in harsh environments.

Moreover, the consideration of low-voltage nearshore grids is motivated by the need for further commercialization of marine current power. With smaller turbines located closer to the shoreline or in rivers, it can be envisioned that the production and deployment of the turbines will be easier and less expensive compared to large turbines deployed in deeper waters farther from the shoreline. The series production of this type of system can lead to economies of scale and provide a much-needed boost to the commercialization of marine current energy.

The system considered in this paper is based on a MCEC developed and deployed by researchers at Uppsala University, Sweden. The turbine is a vertical axis turbine with the generator and turbine mounted on the same axis. The turbine is built to stand on the sea or river bed. From the turbine, an approximately 200 m long three-phase cable connects it with a grid connection system, which is based on a back-to-back converter technology. More information about the turbine and the test site can be found in Refs. [21,22].

A simulation model developed for the system at the test site is presented in Refs. [23,24]. The study presented in this paper is a continuation of the development of the simulation model. The model is used to evaluate three types of DC collection grids consisting of ten turbines. The three considered grid layouts are the series, parallel, and star topologies. The main contribution of the study is the consideration of the collection grid topologies for the specific MCEC technology developed by Uppsala University.

The rest of the paper is organized as follows. In Section 2, the DC grid topologies considered in the study are presented. In Section 3, the MCEC and the model of the system used in the study are presented. This section is mainly based on what has been presented in Refs. [23,24]. The specific model considerations for the study in this paper are presented in Section 4. In Section 5, the results from the simulations are presented, and in Section 6 the topologies are compared. Finally, the conclusions are given in Section 7.

2. DC collection grid topologies

As has already been mentioned, the available research into DC collection grids for offshore applications mainly has a focus on wind power. The topologies presented in this section are, therefore, based on research in offshore wind power.

DC collection grids can be categorized based on how the turbines are electrically connected to the grid. The turbines can be connected electrically in parallel or series to the grid [16,25–29]. Moreover, hybrid typologies can be considered, such as connecting multiple series-connected turbines in parallel. Furthermore, it can also be considered that a substation should be included in the system in which multiple turbines can be interconnected. The purpose of a substation can simply be to connect multiple turbines to a single offshore point and transmit the power to the shore in a single cable. The substation can also have a more active function, such as increasing the voltage for the transmission of power to the shore.

Different advantages and disadvantages of the topologies can be highlighted depending on the specific project, but some general characteristics can be observed. The parallel DC collection grid can be beneficial from the point of view of redundancy. As long as the main cable is intact, the loss of one or more turbines will not affect the transmission of power to the shore from the turbines still in operation. On the other hand, if a turbine is disconnected in the series connected grid, the ability of the grid as a whole to transmit power can be affected if the broken turbine cannot be bypassed, which would require switchgear equipment [13]. A benefit of the series DC grid is that a high DC transmission voltage can be achieved without the need for high voltage boosting capability in the turbines or external substations [16]. The transmission voltage will be the sum of the output voltage from the turbines connected in series. Therefore, even if the output voltage from the individual turbines is below the HV level, HVDC transmission can be achieved by series connecting many turbines. However, a problem with this approach is that some of the turbines will be exposed to a very high voltage, which will make the electrical insulation a more complicated task.

Moreover, a system of series-connected turbines will be sensitive to the voltage variations of the individual turbines [30]. If the output voltage of the turbines cannot be maintained at the desired value, the transmission voltage will fluctuate. If HVDC is to be achieved in the parallel collection grid, a significant DC voltage boosting will be required, which can prove to be a complicated and expensive task. Therefore, it may be necessary to include a substation in the system in which a DC to HVDC conversion is performed. However, in offshore wind farms with HVDC transmission to the shore, the platform with the AC to HVDC equipment is often a very expensive component [31,32]. Consequently, a substation for DC to HVDC conversion can potentially be associated with high costs, significantly increasing the overall cost of the project.

In the study presented in this paper, three types of DC collection grids are considered. The topologies are presented in the following sections. The reasoning behind the design choices will be given. One principle has been governing when designing the systems: using components and systems that correspond to what has been used at Uppsala University's MCEC test site (see Section 3). Since the aim of the study has been to design DC collection grids for marine current power, it can be argued that the validity of the proposed systems is enhanced if the design is based on components and systems that have actually been constructed and experimentally verified.

Since the focus of the study is on the electrical system, the actual spatial placement of the turbines and any potential hydrodynamic interaction between turbines are disregarded. Therefore, in the following presentation, the distance between the turbines refers to the cable length and not the actual location of the turbines.

2.1. Series collection grid

A series DC collection grid is shown in Fig. 1. To clarify the concept, the collection grid is illustrated with three MCECs. The number of turbines can be increased or decreased, but in the design presented in this article, ten turbines are considered. Starting from the external grid (for example, the distribution grid), the AC voltages and currents are transformed to DC by the grid-side converter. The grid-side converter is responsible for maintaining the voltage level of the DC grid (see Section 3.5.2 for more details about the grid-side converter). A cable connects the grid-side converter to the first MCEC. Since the voltage is in DC, it is arguably reasonable to model the cable as a completely resistive component. However, in order to not miss any effects the inductive and capacitive properties of the cables may have on the system, the cable is modeled using a pi equivalent cable model with resistance, inductance, and capacitance. The cable enters and exits the MCEC and then continues in the same manner to the last MCEC in the series. From the last MCEC, a cable is connected to the grid-side converter. This cable could potentially be discarded if the water were to be used as a return conductor, as is sometimes done in HVDC transmission [33].

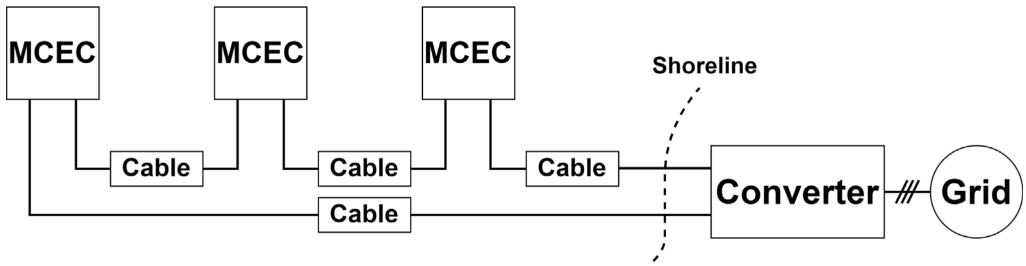

Fig. 1. Series DC collection grid illustrated with three MCECs.

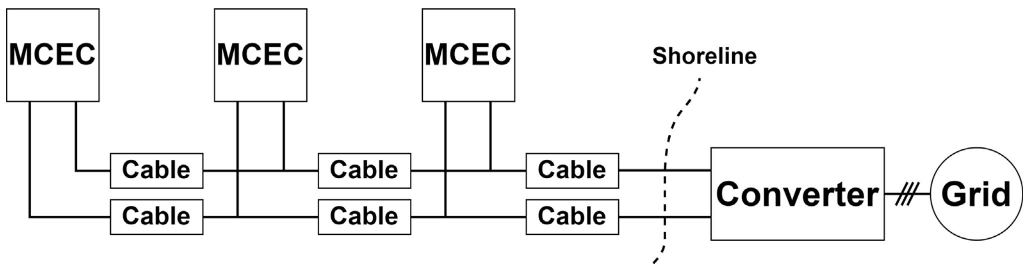

Fig. 2. Parallel DC collection grid illustrated with three MCECs.

The cables between the turbines are assumed to be 20 m, which corresponds to just over three times the diameter of a turbine. Moreover, the first turbine is assumed to be located at a cable length of 200 m from the shore. Consequently, the length of the return conductor is the sum of the cable length between the turbines and the length of the cable from the grid-side converter to the first turbine, which sums up to 380 m. The per meter values of the resistance, capacitance, and inductance are given in Table A.4 in the Appendix.

The DC voltage of the grid is assumed to be maintained by the grid-side converter (in Section 3.5.2, the control method for this function is presented). It would be possible to consider that the MCECs would have a role in maintaining the DC link voltage, which is an approach that has been explored for offshore wind power in Refs. [34,35]. However, since an issue with a series-connected collection grid is the voltage stability at the turbines [30], exploring other concepts of constructing a DC collection grid is of interest. Furthermore, using the grid-side converter to control the DC link voltage in a back-to-back converter is an established concept. However, an issue with this approach is the following. According to Kirchhoff's voltage law, the sum of the voltage drops over the turbines and cable segments must be equal to the voltage over the grid-side converter. Therefore, if all turbines are to deliver power, the voltage reference at the grid-side converter must be set to such a high value that the voltage over the individual turbines becomes large enough. If this is not achieved, some of the turbines will not be able to deliver power to the DC grid. It should also be observed that since the turbines are connected in series, the same current will flow in all parts of the system.

Since the turbines are connected to a single cable in series, the system is sensitive to cable errors. If the cable is broken at any point in the system, the circuit is not closed. This means no power can be delivered from the system, except if an alternative cable is available or the sea is used as a return conductor.

2.2. Parallel collection grid

A parallel DC collection grid is shown in Fig. 2. Again, the system is illustrated with three turbines. From the grid-side converter, two cables are connected to the first MCEC, which is, in turn, connected in parallel to the two cables. This process is repeated for up to the number of turbines that are included in the grid. The cable length from the grid-side converter to the first turbine is assumed to be 200 m, and the length of the cables between the turbines is 20 m.

The grid-side converter is responsible for maintaining the voltage of the grid. The currents in the cable segments will vary in magnitude depending on the specific part of the system under consideration, which is due to Kirchhoff's current law. The 200 m cables will carry the total current, while the last cables will only need to be dimensioned for the current from the last turbine. Furthermore, since the current will give rise to a voltage drop over the cables, the voltage increases incrementally from one turbine to the next, as seen from the grid-side converter.

As long as the cable between the first turbine and the grid-side converter remains intact, the system should, in theory, be able to handle a cable break without a complete loss of power from the farm. For example, if the cable between the last and middle turbine breaks, only the last turbine will be disconnected. The other two turbines should still be able to deliver power to the distribution grid.

2.3. Star collection grid

A star collection grid is shown in Fig. 3. Again, as for the series and parallel collection grids, the star collection grid is illustrated with three turbines. The use of the name "star" to designate the grid derives from the fact that the grid can visually be illustrated in a star-shaped fashion. In the star collection grid, two cables connect the grid-side converter to a hub located in the water. Various choices are available for the hub, ranging from a completely passive component, such as a busbar, to a more active function like voltage boosting.

Furthermore, the hub can be designed as a submerged structure or positioned above sea level. It can be floating or mounted on a bottom-fixed structure, and may also be equipped with measurement and switchgear equipment. In the study presented in this paper, the hub is assumed to be a completely passive component, consisting solely of an equipotential busbar. The turbines are connected to the hub via cables.

The hub is assumed to be connected to the grid-side converter by two 200 m cables, and the turbines are connected to the hub by two 20 m cables. The cables to the shore need to be rated for the complete system, while the cables to the turbines only need to be rated for one turbine. Moreover, as long as the cable from the hub is intact, the farm will be able to supply the distribution grid with power, even if one or more turbines are disconnected.

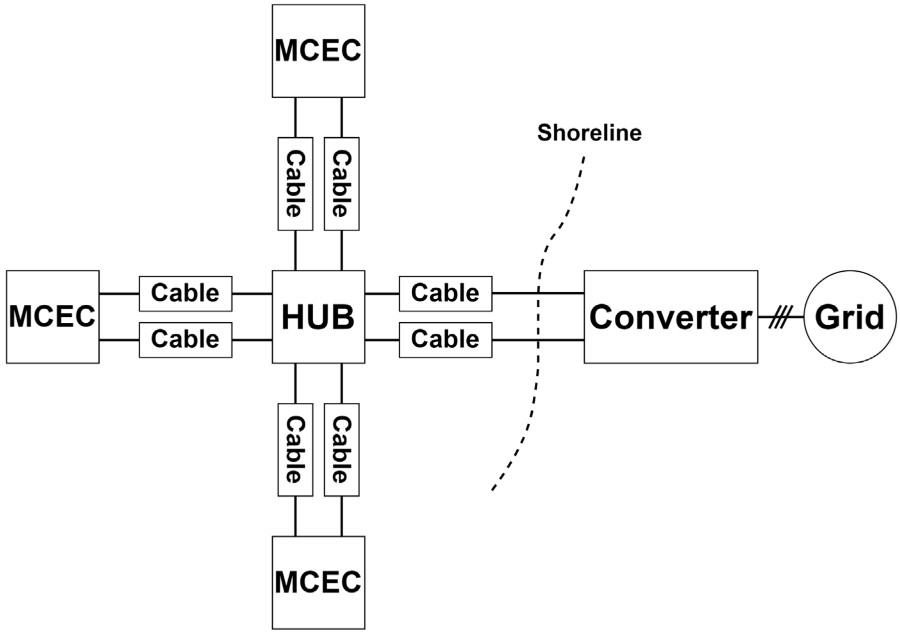

Fig. 3. Star DC collection grid illustrated with three MCECs.

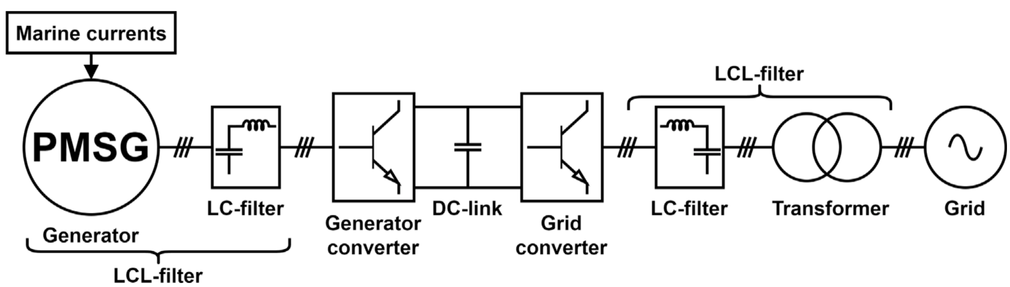

Fig. 4. Overview of the electrical system at the MCEC test site.
Source: Adapted with permission from [24].

3. The marine current energy converter

As has been mentioned, the MCEC considered in this study is the vertical axis turbine developed by researchers at Uppsala University in Sweden. The turbine was deployed in the river Dalälven in Sweden in 2013 [22]. A simulation model has been developed for the system. In this section, an overview of the simulation model is provided. More details of the simulation model and its implementation can be found in Refs. [23,24].

3.1. Overview of the system

An overview of the electrical system at the MCEC test site is shown in Fig. 4. The system is based on a back-to-back converter. The power in the marine currents is transformed to electrical power by the turbine and the generator, which is of the type permanent magnet synchronous generator (PMSG). The AC power from the generator is transmitted to the shore by an approximately 200 m long three-phase cable. On land, the grid connection system is located in a measurement cabin. The AC power from the generator is filtered with an LC filter before being converted to DC by a 2-level voltage source converter (2L-VSC). It should be observed that the LC filter and the inductance of the generator form an LCL filter. The 2L-VSC on the generator side is connected via a DC link to a 3-level voltage source converter (3L-VSC), which in turn is connected to the distribution grid through an LC filter and a power transformer. The LC filter and power transformer form an LCL filter, a concept thoroughly investigated in [36].

3.2. Model assumptions

In the study presented in this article, the system in Fig. 4 is used as a reference for the design. The benefit of this is that the system has been experimentally verified. Therefore, the designs considered in this paper can arguably be more plausible since they are based on systems that have been proven to work.

The DC topologies in Section 2 are evaluated in this paper. To do this, the system in Fig. 4 is split into two parts:

- The generator side, which includes the generator-side converter (the 2L-VSC), the LC filter, the generator and the turbine (which is represented by a hydrodynamic model presented in Section 3.3).
- The grid side, which comprises the grid-side converter (the 3L-VSC), the LC filter, the power transformer and the distribution grid.

The components of the generator side of the system are assumed to be contained either in the turbine or in direct proximity to the turbine. Furthermore, it is assumed that there is no hydrodynamic coupling between the turbines.

3.3. Hydrodynamic model

A marine current turbine converts the energy in the free-flowing water to mechanical energy, which, in turn, is transformed into electrical

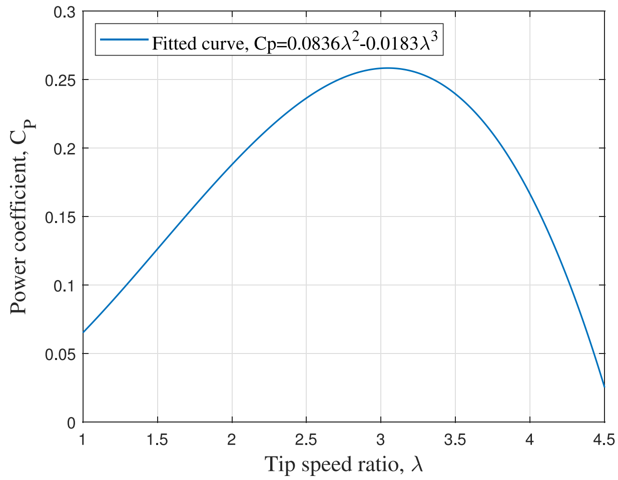

Fig. 5. Power coefficient (C_p) curve fitted from measurements [37]. Optimal tip speed ratio derived from the fitted curve is $\lambda_{opt} \approx 3.05$, which corresponds to an optimal power coefficient of $C_p(\lambda_{opt}) \approx 0.26$.
Source: Reproduced with permission from [23].

energy by the generator. The power in the free-flowing water is given by the following equation:

$$P_w = \frac{1}{2} A \rho_w V_w^3, \tag{1}$$

where A is the swept area of the turbine, ρ_w is the density of water, and V_w is the water speed.

Only a fraction of the power in the free-flowing water is captured by the turbine, given by

$$C_p(\lambda) = \frac{P_t}{P_w}, \tag{2}$$

where $C_p(\lambda)$ is the power coefficient and P_t is the power of the turbine. For a turbine with fixed blades, the power coefficient is only dependent on the tip speed ratio (TSR or λ), defined as the ratio between the tangential speed of the tip of the turbine blade and the speed of the free-flowing water, given by the following equation:

$$\lambda = \frac{\omega_t r}{V_w}, \tag{3}$$

where ω_t is the rotational speed of the turbine, and r is the radius of the turbine.

The power of the turbine can also be expressed in terms of a rotating body as $P_t = \omega_t T_M$, and if combined with Eqs. (1) and (2), the torque on the turbine can be expressed by the following equation:

$$T_M = \frac{1}{2} \frac{A \cdot \rho_w \cdot V_w^3 \cdot C_p(\lambda)}{\omega_t}. \tag{4}$$

The power coefficient curve for the turbine has been evaluated experimentally for TSR values ranging from 2.9 to 4.5 at water speeds ranging from 1.2 m/s to 1.4 m/s in [37]. A curve fitted to the measurement data is given by the following equation:

$$C_p(\lambda) = 0.0836\lambda^2 - 0.0183\lambda^3. \tag{5}$$

The curve of Eq. (5) is shown in Fig. 5.

The hydrodynamic model is shown in Fig. 6. The input parameters to the system are the water speed (V_w) and the rotational speed of the turbine (ω_t). The TSR is calculated using Eq. (3), which, in turn, is used in Eq. (5) to calculate the power coefficient. Finally, the torque is calculated using Eq. (4).

It should be noted that the torque of a vertical axis turbine is associated with fluctuations [38,39]. In the presented hydrodynamic model, there are no fluctuations in the applied torque to the generator. However, since the focus of the study is on the electrical system, this is seen as a satisfactory simplification. Since the power coefficient is based on measurements of the actual turbine, the model will capture the essential behavior of the turbine.

3.4. Drive train model

For the drive train, a simplified one-mass model is used, which is given by the following equation:

$$\frac{d\omega_t}{dt} J = T_M - T_e, \tag{6}$$

where J is the total inertia of the system (in this case, the turbine and the generator), and T_e is the electromagnetic torque. From Eq. (6), it can be observed that by controlling the relationship between the mechanical torque and the electromagnetic torque, the speed of the turbine can be controlled. If $T_M = T_e$, then $\frac{d\omega_t}{dt} = 0$, which means that the turbine is in a steady state. However, if $T_M > T_e$, then $\frac{d\omega_t}{dt} > 0$, and the turbine will accelerate. On the other hand, if $T_M < T_e$, then $\frac{d\omega_t}{dt} < 0$, and the turbine will decelerate.

It should be noted that in the implemented model, a small viscous damping term is also included in Eq. (6). Furthermore, as has already been mentioned, the drive train model is very basic. More complicated higher-order mass models can be considered [40]. In [41], a two-mass drive train model is used for vertical axis wind power turbines. However, since the focus of the study in this paper is on the electrical system, a one-mass representation of the system is deemed adequate.

3.5. Electrical model

An overview of the electrical system will be given in this section. The parameter values used in the model can be found in the Appendix.

3.5.1. Generator side

The generator side of the electrical system is shown in more detail in Fig. 7. In the implemented DC collection grids, this part of the system corresponds to the boxes designated as ”MCEC” in Figs. 1, 2, and 3. The generator side of the system is consequently responsible for rectifying the AC output from the generator and for controlling the generator.

As mentioned earlier, the generator is of the type PMSG, and the torque to the generator is calculated using the hydrodynamic model presented in Section 3.3.

The implemented control method of the PMSG is field-oriented control (FOC) with zero d-axis current. This control method is based on transforming the currents of the generator from a static to a rotating frame of reference in order to have two DC quantities that can be controlled using traditional PI controllers. This type of transformation is often called abc to dq transformation, where the dq-components are used to control the system. In the FOC method, one control loop is used to control the d-axis current, and one control loop is used to control the q-axis current. If the d-axis current is controlled to be zero, it can be shown that the electromagnetic torque is given by the following equation [42]:

$$T_e = \frac{3}{2} p \psi i_{qs}, \tag{7}$$

where ψ is the rotor flux linkage, p is the number of pole pairs, and i_{qs} is the q-axis component of the stator current. If the rotor flux linkage is assumed to be constant, then it can be concluded that a direct relationship exists between the q-axis current and the electromagnetic torque. Consequently, by comparing Eq. (7) with Eq. (6), it can be concluded that the rotational speed of the turbine can be controlled with the q-axis current.

To determine the reference value for the q-axis current, a maximum power point tracking (MPPT) method is employed, as illustrated in the MPPT block in Fig. 7. The implemented MPPT method is the so-called optimal TSR (OTSR) method [43]. This method is very rudimentary, but it requires knowledge of the optimal power coefficient with the

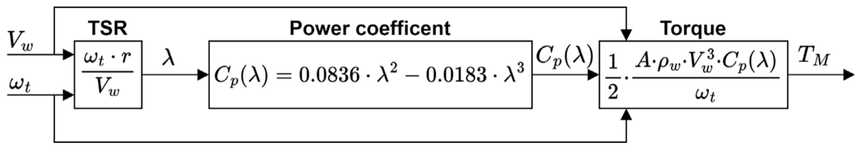

Fig. 6. Hydrodynamic model of the turbine at the test site.

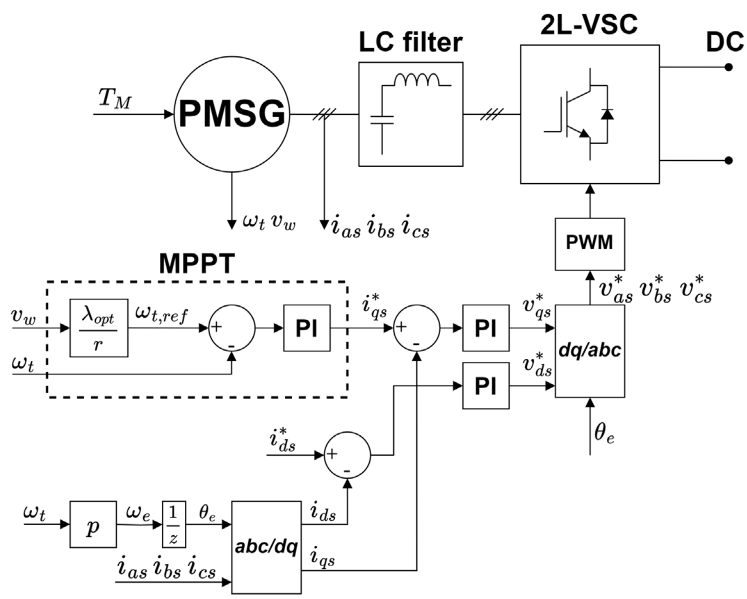

Fig. 7. The generator side of the back-to-back converter.
Source: Adapted with permission from [24].

corresponding optimal TSR, and accurate measurements of the water speed and the rotational speed of the turbine.

From Eq. (5), the optimal power coefficient can be calculated as $C_p(\lambda_{opt}) = 0.26$ at $\lambda_{opt} = 3.05$. Regarding water speed measurements, obtaining accurate measurements of wind speed in wind turbine applications is considered a challenging task [44]. A similar level of complexity can be expected in marine current measurement applications. In the implemented model, however, it is assumed that accurate measurements of water speed are accessible.

In the OTSR method, the optimal value of the TSR is used together with the water speed in Eq. (3) to calculate a reference for the rotational speed of the turbine ($\omega_{t,ref}$). The calculated reference value is compared with the actual rotational speed (ω_t), and the resulting error is sent to a PI controller, which generates a reference value for the q-axis current (i_{qs}^*).

The generator side also comprises an LC filter, which, combined with the inductances of the PMSG, forms an LCL filter. LC filters and LCL filters are associated with resonance issues, which can negatively affect the controller [45]. A passive damping method can be used to mitigate the resonance issue, where resistors are placed in series with the capacitors in the LCL filter [45]. A value for the damping resistor can be calculated using the following equation [46]:

$$R_d = \frac{1}{3\omega_{res} C_f}, \tag{8}$$

where C_f is the filter capacitance, and ω_{res} is the resonance frequency of the filter. If the LCL filter is assumed to be ideal, that is, all resistive components are disregarded, then the resonance frequency can be calculated using the following equation:

$$\omega_{res} = \sqrt{\frac{L_1 + L_2}{L_1 L_2 C_f}}, \tag{9}$$

where L_1 and L_2 are the inductances of the LCL filter.

Using Eq. (8) and (9) with the parameter values in the Appendix, the resistance value can be calculated to 3.49 Ω. Since the real system includes many resistive parts that are not included in the model, such as the resistance of cables and connectors, the damping resistor can, to some extent, be said to compensate for these unknown resistances.

3.5.2. Grid side

The side of the back-to-back converter connected to the external distribution grid is shown in Fig. 8. In the DC collection grids depicted in Figs. 1, 2, and 3, this part corresponds to the block designated as the "Converter". The functions of the grid-side converter are to maintain the DC link voltage at a predefined value and inject the power from the DC grid into the external AC grid.

The external AC grid is assumed to have a line-to-line voltage of 400 V and a frequency of 50 Hz. The external grid is modeled non-ideal with a line resistance of 34 mΩ and a line inductance of 0.5 mH [47].

The 3L-VSC is controlled using voltage-oriented control (VOC) with a phase-locked loop (PLL) method. The purpose of the PLL method is to synchronize the VOC with the grid voltage angle (θ_g). The selected PLL method is the synchronous reference frame PLL (SRF-PLL) method, which the interested reader can read more about in Ref. [48].

Similar to the generator-side controller, the VOC is based on a transformation of the currents and voltages from a static frame of reference to a synchronous reference frame, that is, an abc to dq transformation. A decoupled controller with two PI controllers is then used to generate reference dq voltages, which are used to create control signals for the VSC. The controller being decoupled means that the d and q components can be controlled independently of each other. This, in turn, allows for the independent control of reactive and active power exchanged with the AC grid. An outer control loop consisting of a PI controller is used to control the DC link voltage by comparing the set point value of the DC voltage (v_{dc}^*) with the actual DC voltage (v_{dc}) and generating a reference value for the d-axis grid current (i_{dg}^*).

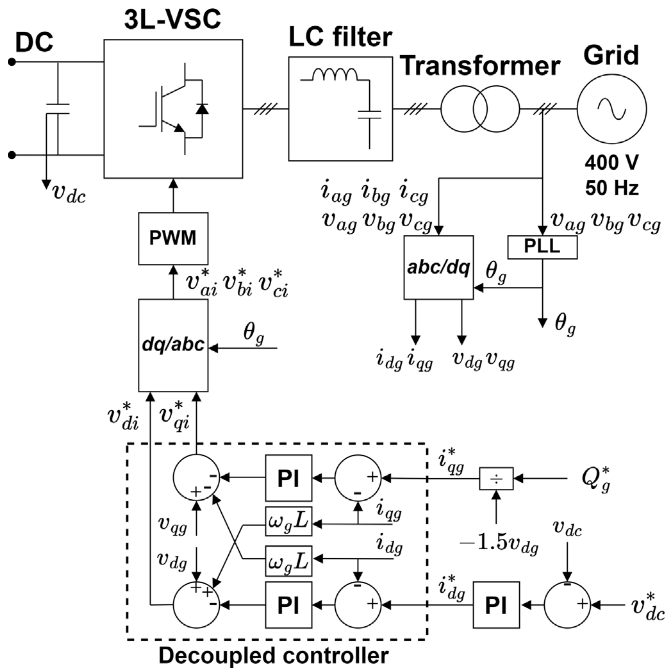

Fig. 8. The grid side of the back-to-back converter.
Source: Adapted with permission from [24].

As noted earlier, the LC filter and the inductance of the power transformer form an LCL filter. Similar to the generator-side LCL filter, the grid-side filter is associated with resonance issues, which can have adverse effects on the control system. In order to mitigate these issues, a passive damping strategy is used in which resistors are connected in series with the capacitors in the LC filter. In [36], a modified version of Eq. (9) is presented for specifically this design of the grid connection system. Using the modified equation, together with Eq. (8), and the parameter values in the Appendix, the value of the damping resistor is calculated to 2.31 Ω. Again, since many resistive parts of the system are not included in the model, such as the resistance of connectors and jumper cables, the damping resistor can also partly be viewed as introducing a representation of unknown resistances in the system.

4. Simulation model

The model presented in the previous sections was implemented in MATLAB/Simulink (version: R2022a). The PMSG was implemented using the built-in permanent magnet synchronous machine block. The electrical components were implemented using the Powergui components. The PI controllers were of the type discrete parallel controllers, and the gains of the controllers were set by trial and error. The solver settings in Simulink were fixed-step with automatic solver selection (in all simulation cases in this study, the resulting solver was "ode3"). The fixed-step size (fundamental sample time) was set to 1 µs.

The systems were implemented with ten turbines; the cable distance between the turbines has already been discussed in Section 2 but is also summarized in Table 1. In this table, the considered DC voltages are also included. For the parallel and star collection grids, DC voltages of 400 V and 600 V are considered. For the series connected collection grid, DC reference voltages of 600 V and 2000 V are considered.

It is reasonable to assume that the water speeds at the turbines may differ due to factors such as hydrodynamic coupling between the turbines or the effects of the terrain. Therefore, from the perspective of evaluating system performance, it is suitable to consider a range of water speeds. Consequently different water speeds are applied to the turbines, but the same values are used in all simulations. The water speeds are selected to values around the nominal water speed of 1.3 m/s: $v_{w,T_1} = 1.21$ m/s, $v_{w,T_2} = 1.33$ m/s, $v_{w,T_3} = 1.31$ m/s, $v_{w,T_4} = 1.25$ m/s, $v_{w,T_5} = 1.18$ m/s, $v_{w,T_6} = 1.35$ m/s, $v_{w,T_7} = 1.36$ m/s, $v_{w,T_8} = 1.41$ m/s, $v_{w,T_9} = 1.38$ m/s, and $v_{w,T_{10}} = 1.22$ m/s.

Table 1
Grid parameters for the considered DC collection grid topologies.

Parameters	Series grid	Parallel grid	Star grid
Number of turbines.	10	10	10
DC voltages.	600 V & 2000 V	400 V & 600 V	400 V & 600 V
Cable length between the turbines, and the hub and the turbines.	20 m	20 m	20 m
Cable length from the grid-side converter to the first turbine, and the hub.	200 m	200 m	200 m
Cable length from the last turbine in a row and the grid-side converter.	380 m	–	–

The implications of varying water speeds can be understood by observing Eq. (1), which shows that the power converted to mechanical power by the turbine is highly affected by the water speed, specifically by the cube of the water speed. An initial observation is that differences in power will have implications for the voltage and current from the generator. Depending on the specific configuration of the DC grid, this will then have implications for the voltage and current from a turbine connecting to the grid. For example, if a parallel DC grid with a fixed voltage level is considered, the turbines connecting to the grid will inject currents of different sizes depending on the difference in water speed. It may be necessary to consider this in the design process to avoid unexpected issues related to robustness of the system, such as the correct rating of the components.

5. Results from simulations of the topologies

In this section, the results from the simulations are presented. The emphasis is on the DC voltages and the ability of the system to inject power into the distribution grid.

5.1. Series DC collection grid

The series DC collection grid was simulated with a voltage reference of 600 V and 2000 V. The system was simulated for 50 s.

Fig. 9 shows the DC voltages at the turbines and the grid-side converter. If the voltages for the situation when the DC voltage reference is 600 V in Fig. 9(a) are considered, it can first be observed that the voltages of some of the turbines go to a value close to zero a very short time after the simulation is started. Moreover, the rotational speeds of the turbines are shown in Fig. 10, and from Fig. 10(a), it can be seen that five turbines, namely turbines 1, 3–5, and 10, have a rotational speed of almost zero, indicating that the turbines have stopped. It can also be observed from Fig. 10(a) that the rotational speeds of the turbines that are still operating show large variations.

The issue here is that the DC voltages across the turbines become too small for the controllers in the turbines to operate correctly, and this forces the turbines to stop. To be more precise, the low DC voltage means that the generator VSC operates far in the overmodulation region [49], resulting in the controller not operating correctly. For the turbines with the lowest water speed, this results in the complete failure to operate, while the turbines with higher water speeds can still operate, albeit under very unstable conditions.

In Fig. 11(a), the TSR for the series grid with a voltage reference of 600 V is shown. The TSR is calculated using Eq. (3), and the presence of the rotational speed (ω_t) in the equation means that the same tendencies as for the rotational speed are seen in the TSR; namely, the turbines that have a rotational speed of almost zero also attain a TSR

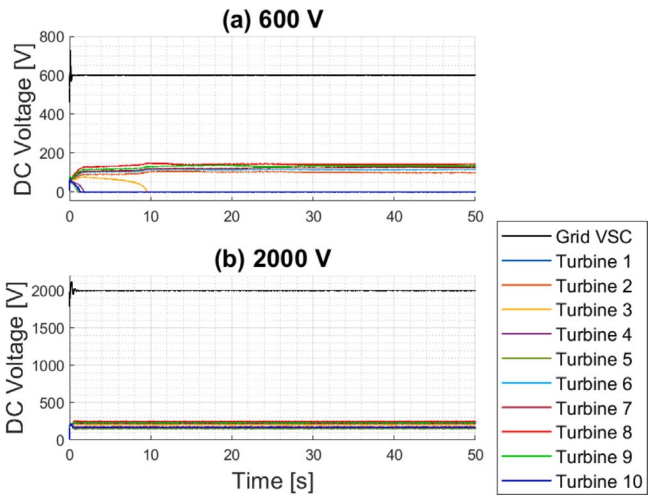

Fig. 9. The voltages at the turbines and the grid-side converter for the series DC collection grid with (a) a reference DC voltage of 600 V, and (b) a reference DC voltage of 2000 V.

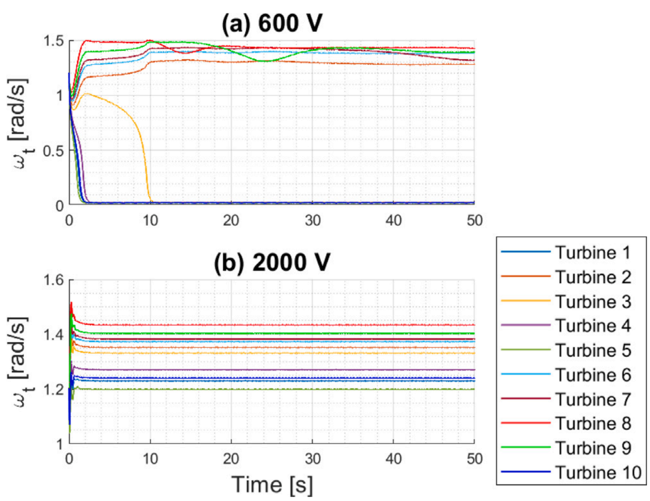

Fig. 10. The rotational speed of the turbines for the series DC collection grid with (a) a reference DC voltage of 600 V, and (b) a reference DC voltage of 2000 V.

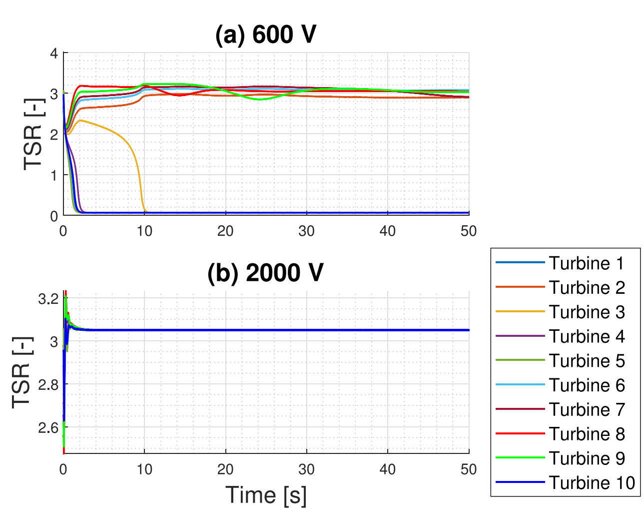

Fig. 11. The TSR for the turbines in the series DC collection grid with (a) a reference DC voltage of 600 V, and (b) a reference DC voltage of 2000 V.

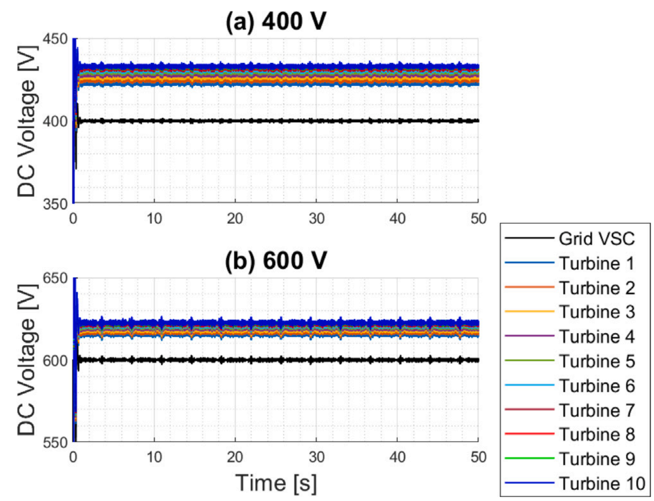

Fig. 12. The voltages at the turbines and the grid-side converter for the parallel DC collection grid with (a) a reference DC voltage of 400 V, and (b) a reference DC voltage of 600 V.

of zero. None of the turbines that are able to supply power to the grid are operating at the optimal TSR.

In order to assess the system when all turbines operate, the reference voltage was increased to 2000 V. Disregarding the voltage drops over the cable segments and assuming an equal distribution of the voltages over the turbines, a voltage drop of 200 V over each turbine would be expected. Since the rated voltage of the generator is 138 V (see Appendix), this would place the generator VSC just above the overmodulation limit. However, as observed in Fig. 9(b), the reference voltage of 2000 V is sufficiently high to ensure the correct operation of all turbines. The reason behind this is that some of the turbines operate at a water speed below the rated value. The DC voltages range from 152 V for the turbine with the lowest water speed to 250 V for the turbine with the highest water speed. From Fig. 10 and Fig. 11, it can be concluded that all turbines achieve stable operation regarding the rotational speed and that the MPPT controller is able to steer all turbines to the optimal TSR of 3.05.

5.2. Parallel DC collection grid

The parallel DC collection grid was simulated with reference voltages of 400 V and 600 V. The system was simulated for 50 s.

In Fig. 12, the DC voltages are shown. As can be seen, the controller is able to achieve the reference value of 400 V in Fig. 12(a) and 600 V in Fig. 12(b). In both cases, it can be observed that the voltages at the turbines are higher than the voltage at the grid-side converter. The reason for this is that the voltage drop over the cables forces the voltages at the turbines to a higher value. As is visible in the figure, the voltage at turbine 10, that is, the last turbine in the row, is at the highest voltage.

The rotational speeds of the turbines are shown in Fig. 13. As can be seen, all turbines are able to achieve stable operation. Moreover, the TSR for the turbines is shown in Fig. 14. All turbines operate at the optimal TSR of 3.05.

It can consequently be concluded that the parallel DC collection grid is able to achieve stable operation at the optimal TSR for both reference voltages of 400 V and 600 V.

5.3. Star DC collection grid

The star DC collection grid was simulated with voltage reference values of 400 V and 600 V. The system was simulated for 50 s.

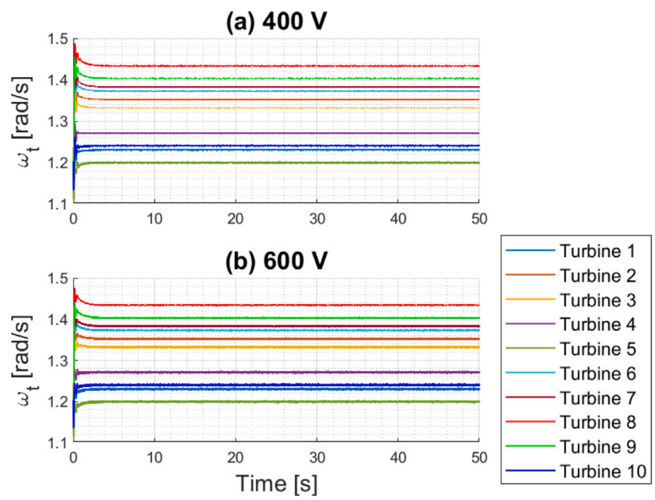

Fig. 13. The rotational speed of the turbines for the parallel DC collection grid with (a) a reference DC voltage of 400 V, and (b) a reference DC voltage of 600 V.

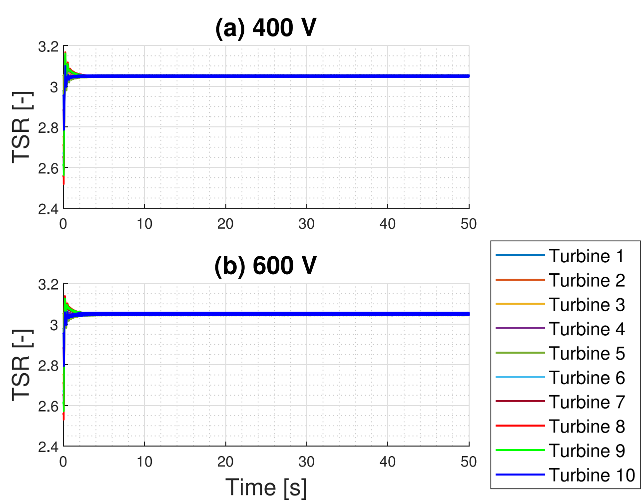

Fig. 14. The TSR for the turbines in the parallel DC collection grid with (a) a reference DC voltage of 400 V, and (b) a reference DC voltage of 600 V.

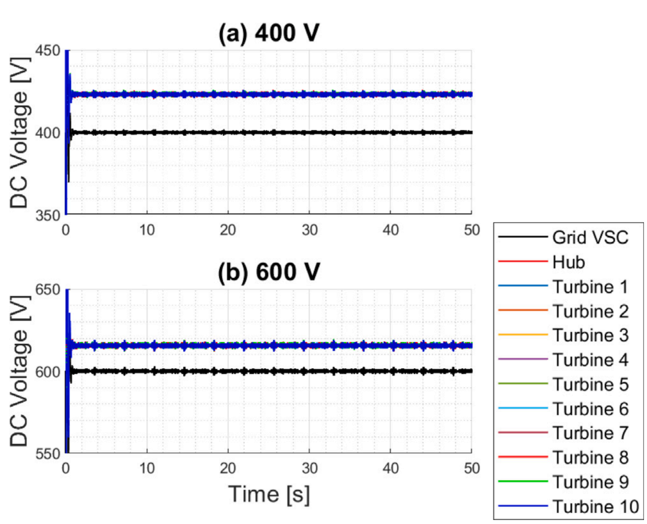

Fig. 15. The voltages at the turbines, the hub, and the grid-side converter for the star DC collection grid with (a) a reference DC voltage of 400 V, and (b) a reference DC voltage of 600 V.

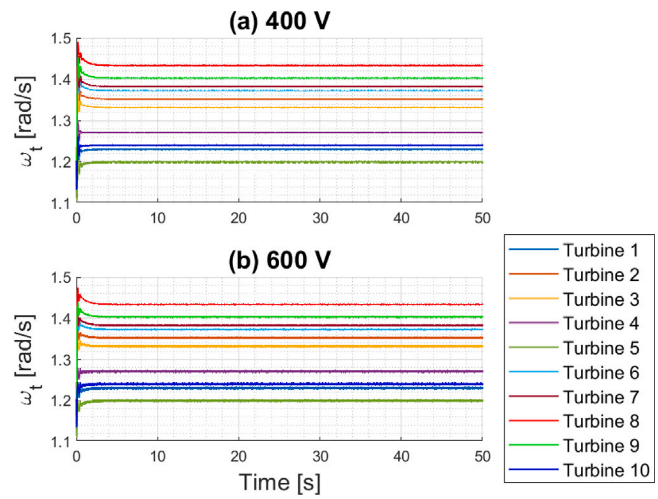

Fig. 16. The rotational speed of the turbines for the star DC collection grid with (a) a reference DC voltage of 400 V, and (b) a reference DC voltage of 600 V.

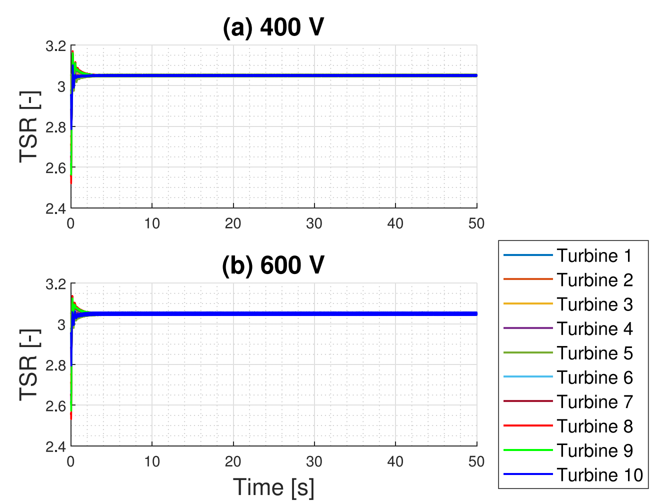

Fig. 17. The TSR for the turbines in the star DC collection grid with (a) a reference DC voltage of 400 V, and (b) a reference DC voltage of 600 V.

The DC voltages are shown in Fig. 15. The system exhibits the same general behavior for both the case with 400 V and 600 V. The grid-side converter is able to maintain the reference voltage. The voltage at the hub is at a higher level because of the voltage drop over the cable from the hub to the grid-side converter. However, it should be noted that since the cables from the individual turbines are short and only a modest current passes through the cables, the voltage difference between the turbines and the bus in the hub is only very minor, at the decimal level. Therefore, the individual turbine voltages and the hub voltage are indistinguishable in Fig. 15. The DC voltage at the hub and the turbines are approximately 423 V for the system with a reference voltage of 400 V and approximately 616 V for the reference value of 600 V.

If the rotational speed of the turbines in Fig. 16 and the TSR in Fig. 17 are considered, it can be concluded that the controller can achieve stable operation of the turbine speed in the star collection grid as well, and the MPPT control can steer the turbine towards the optimal TSR value of 3.05.

6. Comparison of the topologies

Table 2 shows the power injected into the AC distribution grid from the considered topologies. The power is calculated as the mean value of

Table 2
Mean power injected into the distribution grid for the series, parallel, and star DC collection grids at various reference voltages.

Voltage	Series	Parallel	Star
400 V	–	39.45 kW	39.98 kW
600 V	23.12 kW	40.17 kW	40.44 kW
2000 V	40.80 kW	–	–

the power injected into the AC grid for the last 20 s of the simulation. It can first be noted that the series DC collection grid with a voltage reference of 600 V is an obvious outlier, only injecting almost half of the power of the other DC grid topologies. This is, of course, due to the fact that only five of ten turbines are operational. For the other topologies, the power injected into the AC grid is around 40 kW. The power increases with the increase of the DC voltage reference, which is expected because a higher voltage means the current will be smaller, and therefore, also the ohmic losses. The lowest losses are seen in the DC series system with a voltage reference of 2000 V, in which the power injected into the grid is 40.80 kW. This is closely followed by the DC star system with a voltage reference of 600 V and an injected power into the AC grid of 40.44 kW.

Since the power is very similar in all considered cases, excluding the series 600 V, other factors must be considered in the choice of design. Regarding the series DC grid, stability issues are a pressing concern. The reference voltage needs to be high enough to ensure the turbines do not enter the overmodulation region. On the other hand, a large DC voltage over the grid-side VSC will make this design more complicated; for example, higher-rated components will be required.

The star collection grid is an appealing solution since the hub allows for a degree of modularity; turbines can be added incrementally. Moreover, the system is characterized by a high degree of redundancy. A loss of one or more of the turbines will not affect the supply of power from the rest of the turbines. The only way the whole farm can be affected is by a failure of the cables from the hub to the onshore converter or by a failure of the hub itself. However, the construction of offshore components is often highly complex and associated with high costs. Therefore, decreasing the number of offshore components can be a desirable goal in farm design.

The parallel collection grid can be an interesting option since no offshore hub is needed. Moreover, since the turbines are connected in parallel to the grid, the system will be less sensitive to the loss of an individual turbine. Furthermore, the currents in the system will differ, which means that the different current ratings of the cables can be used. For example, the cable from the first turbine to the onshore converter must be rated for the complete system, while the cable from turbine 9 to 10 only needs to be rated for turbine 10.

7. Conclusions

Three DC collection grid topologies have been considered for a specific MCEC technology: series, parallel, and star collection grids. Simulations have demonstrated that all three topologies are capable of supplying power to the external AC grid. However, the series DC collection grid requires a higher DC collection grid voltage for the control system in the turbines to operate correctly. The lowest losses, or the highest power injected into the AC grid, are achieved by the series collection grid with a DC voltage reference of 2000 V, producing an AC power of 40.80 kW. This is followed by the star collection grid with a power of 40.44 kW at a DC voltage reference of 600 V, and the parallel collection grid with a power of 40.17 kW at a DC voltage reference of 600 V. Since the power difference between the topologies is relatively minor, it is concluded that other factors need to be considered in the choice between the designs. One issue that may need to be considered is the appropriate voltage level. As noted for the DC series grid, if the reference value for the grid voltage is too small, this can lead to the turbines malfunctioning. On the other hand, increasing the voltage level will require more attention to the insulation of the system and higher ratings of the components, which can result in increased costs of the project. Ultimately, a site- and project-specific evaluation will be necessary to account for these factors and other aspects, such as terrain, local regulations, and commercially available components.

Table A.3
Turbine and generator parameters.
Source: The table is adapted from [23,24,47].

Turbine	
$C_p(\lambda_{opt})$	0.26 at $\lambda_{opt} = 3.05$
Type	Vertical axis
Rotor height	3.5 m
Rotor radius (r)	3 m
Turbine area (A)	21 m^2
Generator	
Type	PMSG
Power rating	7.5 kW
Nominal rotational speed	15 rpm
Minimum efficiency	80 %
Number of poles	112
Rated voltage ($V_{LL,rms}$)	138 V
Rated stator current (rms)	31 A
Stator phase resistance	0.335 Ω
Armature inductance	3.5 mH
Flux linkage[a,b]	1.29 Wb
Inertia[b]	2445 kg m^2
Viscous friction coefficient[b]	1 N m s

[a] Assuming a constant flux.
[b] The values for flux linkage, inertia and viscous friction are estimates.

CRediT authorship contribution statement

Christoffer Fjellstedt: Writing – review & editing, Writing – original draft, Visualization, Validation, Software, Resources, Project administration, Methodology, Investigation, Formal analysis, Data curation, Conceptualization. **Johan Forslund:** Validation, Resources, Methodology, Investigation, Data curation, Conceptualization. **Karin Thomas:** Supervision, Project administration, Funding acquisition, Conceptualization.

Declaration of competing interest

The authors declare that they have no known competing financial interests or personal relationships that could have appeared to influence the work reported in this paper.

Data availability

Data will be made available on request.

Acknowledgment

This work was supported by STandUP for Energy

Appendix. System parameters

In Table A.3 and A.4 the parameters used in the study are shown. The tables are adapted from Refs. [23,24,47].

Table A.4
Electrical system parameters.
Source: The table is adapted from [23,24,47].

Component	Parameters	Values
Cable	Resistance	0.524 Ω/km
	Inductance	0.24 mH/km
	Capacitance	0.45 μF/km
Rectifier	Converter type	2L-VSC
	Modulation scheme	SPWM
	Switching frequency	4 kHz
	Harmonic LC filter	1.6 mH, 10 μF
	Damping resistance	3.49 Ω
DC link filter	Capacitor bank	16.5 mF
Inverter	Converter type	3L-VSC
	Modulation scheme	SPWM
	Switching frequency	6 kHz
	Harmonic LC filter	2.4 mH (66 mΩ) 10 μF
	Damping resistance	2.31 Ω
Transformer	Delta/Wye	400 V/230 V
	Power rating	7.5 kVA
	Primary resistance	0.7 Ω
	Secondary resistance	0.23 Ω
	Primary leak. inductance	0.9 mH
	Secondary leak. inductance	0.3 mH
	Magnetization resistance	8225 Ω
	Magnetization inductance	9.22 H
Grid	Three-phase symmetrical	400 V/50 Hz
IGBT	Internal resistance	0.1 mΩ
	Forward voltage	1 V
Rectifier diode	Internal resistance	0.001 Ω
	Forward voltage	0.8 V
Snubber circuit	Snubber resistance	47 kΩ
	Snubber capacitance	470 nF

References

[1] H. Chen, T. Tang, N. Aït-Ahmed, M.E.H. Benbouzid, M. Machmoum, M.E.-H. Zaïm, Attraction, challenge and current status of marine current energy, IEEE Access 6 (2018) 12665–12685, http://dx.doi.org/10.1109/ACCESS.2018.2795708.

[2] A.S. Bahaj, Marine current energy conversion: the dawn of a new era in electricity production, Phil. Trans. R. Soc. A 371 (2013) 20120500, http://dx.doi.org/10.1098/rsta.2012.0500.

[3] R. Samsó, J. Crespin, A. García-Olivares, J. Solé, Examining the potential of marine renewable energy: a net energy perspective, Sustainability 15 (10) (2023) http://dx.doi.org/10.3390/su15108050.

[4] Annual Report: An Overview of Ocean Energy Activities in 2022, Tech. Rep., IEA-OES, 2023.

[5] EnFAIT, 2024, URL https://www.enfait.eu/. (Accessed 09 January 2024).

[6] Z. Li, Q. Song, F. An, B. Zhao, Z. Yu, R. Zeng, Review on DC transmission systems for integrating large-scale offshore wind farms, Energy Convers. Econ. 2 (1) (2021) 1–14, http://dx.doi.org/10.1049/enc2.12023.

[7] E.P. Soares-Ramos, L. de Oliveira-Assis, R. Sarrias-Mena, L.M. Fernández-Ramírez, Current status and future trends of offshore wind power in Europe, Energy 202 (2020) 117787, http://dx.doi.org/10.1016/j.energy.2020.117787.

[8] H. Díaz, C. Guedes Soares, Review of the current status, technology and future trends of offshore wind farms, Ocean Eng. 209 (2020) 107381, http://dx.doi.org/10.1016/j.oceaneng.2020.107381.

[9] F. Blaabjerg, K. Ma, Wind energy systems, Proc. IEEE 105 (11) (2017) 2116–2131, http://dx.doi.org/10.1109/JPROC.2017.2695485.

[10] J. Deng, F. Cheng, L. Yao, J. Xu, B. Mao, X. Li, R. Chen, A review of system topologies, key operation and control technologies for offshore wind power transmission based on HVDC, IET Gener. Transm. Distrib. 17 (15) (2023) 3345–3363, http://dx.doi.org/10.1049/gtd2.12894.

[11] V. Timmers, A. Egea-Àlvarez, A. Gkountaras, R. Li, L. Xu, All-DC offshore wind farms: When are they more cost-effective than AC designs? IET Renew. Power Gener. 17 (10) (2023) 2458–2470, http://dx.doi.org/10.1049/rpg2.12550.

[12] C. Meyer, M. Hoing, A. Peterson, R.W. De Doncker, Control and design of DC grids for offshore wind farms, IEEE Trans. Ind. Appl. 43 (6) (2007) 1475–1482, http://dx.doi.org/10.1109/TIA.2007.908182.

[13] M. De Prada Gil, J. Domínguez-García, F. Díaz-González, M. Aragüés-Peñalba, O. Gomis-Bellmunt, Feasibility analysis of offshore wind power plants with DC collection grid, Renew. Energy 78 (2015) 467–477, http://dx.doi.org/10.1016/j.renene.2015.01.042.

[14] K. Musasa, N.I. Nwulu, M.N. Gitau, R.C. Bansal, Review on DC collection grids for offshore wind farms with high-voltage DC transmission system, IET Power Electron. 10 (15) (2017) 2104–2115, http://dx.doi.org/10.1049/iet-pel.2017.0182.

[15] P. Lakshmanan, J. Liang, N. Jenkins, Assessment of collection systems for HVDC connected offshore wind farms, Electr. Power Syst. Res. 129 (2015) 75–82, http://dx.doi.org/10.1016/j.epsr.2015.07.015.

[16] P. Lakshmanan, R. Sun, J. Liang, Electrical collection systems for offshore wind farms: A review, CSEE J. Power Energy Syst. 7 (5) (2021) 1078–1092, http://dx.doi.org/10.17775/CSEEJPES.2020.05050.

[17] Marine Energy Electrical Architecture - Report 1: Landscape Map and Literature Review, Tech. Rep., CATAPULT Offshore Renewable Energy (CORE), 2015.

[18] Marine Energy Electrical Architecture - Report 2: Review of SSE Contractor Reports , Tech. Rep., CATAPULT Offshore Renewable Energy (CORE), 2015.

[19] Marine Energy Electrical Architecture - Report 3: Optimum Electrical Array Architectures, Tech. Rep., CATAPULT Offshore Renewable Energy (CORE), 2015.

[20] A.J. Collin, A.J. Nambiar, D. Bould, B. Whitby, M.A. Moonem, B. Schenkman, S. Atcitty, P. Chainho, A.E. Kiprakis, Electrical components for marine renewable energy arrays: a techno-economic review, Energies 10 (12) (2017) http://dx.doi.org/10.3390/en10121973.

[21] S.L. Katarina Yuen, M. Grabbe, E. Lalander, A. Goude, M. Leijon, The Söderfors project: construction of an experimental hydrokinetic power station, in: Proc. 9th European Wave and Tidal Energy Conference, EWTEC, Southampton, UK, 2011.

[22] S. Lundin, J. Forslund, N. Carpman, M. Grabbe, K. Yuen, S. Apelfröjd, A. Goude, M. Leijon, The Söderfors project: experimental hydrokinetic power station deployment and first results, in: Proc. 10th European Wave and Tidal Energy Conference, EWTEC, Aalborg, Denmark, 2013.

[23] C. Fjellstedt, J. Forslund, K. Thomas, Simulations of the electrical system of a grid connected marine current energy converter, in: Proc. 14th European Wave and Tidal Energy Conference, Plymouth, UK, 2021.

[24] C. Fjellstedt, J. Forslund, K. Thomas, A comparison of AC and DC collection grids for marine current energy, in: Proc. 15th European Wave and Tidal Energy Conference, Bilbao, Spain, 2023, http://dx.doi.org/10.36688/ewtec-2023-207.

[25] R. Srikakulapu, U. Vinatha, Electrical collector topologies for offshore wind power plants: A survey, in: Proc. 2015 IEEE 10th International Conference on Industrial and Information Systems, ICIIS, Peradeniya, Sri Lanka, 2015, pp. 338–343, http://dx.doi.org/10.1109/ICIINFS.2015.7399034.

[26] S.M. Alagab, S. Tennakoon, C. Gould, Review of wind farm power collection schemes, in: Proc. 2015 50th International Universities Power Engineering Conference, UPEC, Stoke on Trent, UK, 2015, http://dx.doi.org/10.1109/UPEC.2015.7339922.

[27] H.J. Bahirat, B.A. Mork, H.K.H. idalen, Comparison of wind farm topologies for offshore applications, in: Proc. 2012 IEEE Power and Energy Society General Meeting, San Diego, CA, USA, 2012, http://dx.doi.org/10.1109/PESGM.2012.6344689.

[28] S. Lundberg, Wind Farm Configuration and Energy Efficiency Studies: Series DC Versus AC Layouts (Ph.D. thesis), Chalmers University of Technology, 2006.

[29] S. Lundberg, Evaluation of wind farm layouts, EPE Journal (European Power Electronics and Drives Journal) 16 (1) (2006) 14–21, http://dx.doi.org/10.1080/09398368.2006.11463608.

[30] A. Follo, O. Saborío-Romano, E. Tedeschi, N.A. Cutululis, Challenges in all-DC offshore wind power plants, Energies 14 (19) (2021) http://dx.doi.org/10.3390/en14196057.

[31] Electricity Ten Year Statement 2014 (ETYS 2014), Tech. Rep., National Grid ESO, UK, 2014.

[32] Electricity Ten Year Statement 2015 (ETYS 2015), Tech. Rep., National Grid ESO, UK, 2015.

[33] S.J. Sutton, P.L. Lewin, S.G. Swingler, Review of global HVDC subsea cable projects and the application of sea electrodes, Int. J. Electr. Power Energy Syst. 87 (2017) 121–135, http://dx.doi.org/10.1016/j.ijepes.2016.11.009.

[34] N. Holtsmark, H.J. Bahirat, M. Molinas, B.A. Mork, H.K. Hoidalen, An all-DC offshore wind farm with series-connected turbines: an alternative to the classical parallel AC model? IEEE Trans. Ind. Electron. 60 (6) (2013) 2420–2428, http://dx.doi.org/10.1109/TIE.2012.2232255.

[35] M. Guan, A series-connected offshore wind farm based on modular dual-active-bridge (DAB) isolated DC–DC converter, IEEE Trans. Energy Convers. 34 (3) (2019) 1422–1431, http://dx.doi.org/10.1109/TEC.2019.2918200.

[36] C. Fjellstedt, J. Forslund, K. Thomas, Experimental investigation of the frequency response of an LC-filter and power transformer for grid connection, Energies 16 (2023) 5784, http://dx.doi.org/10.3390/en16155784.

[37] S. Lundin, J. Forslund, A. Goude, M. Grabbe, K. Yuen, M. Leijon, Experimental demonstration of performance of a vertical axis marine current turbine in a river, J. Renew. Sustain. Energy 8 (6) (2016) http://dx.doi.org/10.1063/1.4971817, Art. no. 064501.

[38] Z. Zhou, M. Benbouzid, J.-F. Charpentier, F. Scuiller, T. Tang, Developments in large marine current turbine technologies – A review, Renew. Sustain. Energy Rev. 71 (2017) 852–858, http://dx.doi.org/10.1016/j.rser.2016.12.113.

[39] B. Govind, Increasing the operational capability of a horizontal axis wind turbine by its integration with a vertical axis wind turbine, Appl. Energy 199 (2017) 479–494, http://dx.doi.org/10.1016/j.apenergy.2017.04.070.

[40] S.M. Muyeen, M.H. Ali, R. Takahashi, T. Murata, J. Tamura, Y. Tomaki, A. Sakahara, E. Sasano, Comparative study on transient stability analysis of wind turbine generator system using different drive train models, IET Renew. Power Gener. 1 (2) (2007) 131.

[41] M. Rossander, C. Fjellstedt, H. Bernhoff, Multiple vertical axis wind turbines with passive rectification to a common DC-link, Renew. Energy 127 (2018) 1101–1110, http://dx.doi.org/10.1016/j.renene.2018.05.013.

[42] B. Wu, Y. Lang, N. Zargari, S. Kouro, Power Conversion and Control of Wind Energy Systems, first ed., John Wiley & Sons, Hoboken, New Jersey, US, 2011.

[43] D. Kumar, K. Chatterjee, A review of conventional and advanced MPPT algorithms for wind energy systems, Renew. Sustain. Energy Rev. 55 (2016) 957–970, http://dx.doi.org/10.1016/j.rser.2015.11.013.

[44] J.S. Thongam, M. Tarbouchi, R. Beguenane, A.F. Okou, A. Merabet, P. Bouchard, An optimum speed MPPT controller for variable speed PMSG wind energy conversion systems, in: Proc. IECON 2012 - 38th Annual Conference on IEEE Industrial Electronics Society, IEEE, 2012, pp. 4293–4297, http://dx.doi.org/10.1109/IECON.2012.6389199.

[45] C.C. Gomes, A.F. Cupertino, H.A. Pereira, Damping techniques for grid-connected voltage source converters based on LCL filter: An overview, Renew. Sustain. Energy Rev. 81 (2018) 116–135, http://dx.doi.org/10.1016/j.rser.2017.07.050.

[46] S.V. Araujo, A. Engler, B. Sahan, F.L.M. Antunes, LCL filter design for grid-connected NPC inverters in offshore wind turbines, in: Proc. 2007 7th International Conference on Power Electronics, 2007, pp. 1133–1138, http://dx.doi.org/10.1109/ICPE.2007.4692556.

[47] S. Apelfröjd, R. Ekström, K. Thomas, M. Leijon, A back-to-back 2L-3L grid integration of a marine current energy converter, Energies 8 (2015) 808–820, http://dx.doi.org/10.3390/en8020808.

[48] S. Golestan, J.M. Guerrero, J.C. Vasquez, Three-phase PLLs: a review of recent advances, IEEE Trans. Power Electron. 32 (2017) 1894–1907, http://dx.doi.org/10.1109/TPEL.2016.2565642.

[49] N. Mohan, T.M. Undeland, W.P. Robbins, Power electronics: converters, applications and design, in: Power Electronics: Converters, Applications and Design, third ed., Wiley, Hoboken, N.J, 2003.